coatings

MDPI

Article

High Performance Planar Structure Perovskite Solar Cells Using a Solvent Dripping Treatment on Hole Transporting Layer

Xuhui Wang [1], Gang Lu [1,2], Min Zhang [1], Yali Gao [1], Yanbo Liu [1], Long Zhou [3] and Zhenhua Lin [3,*]

1 Qinghai Huanghe Upstream Hydropower Development Co., Ltd., Photovoltaic Industry Technology Branch, Photovoltaic Technology Co., Ltd., of Huanghe Hydropower, Xining 810000, China; wangxuhui@spic.com.cn (X.W.); eelugang@163.com (G.L.); zhangmin@spic.com.cn (M.Z.); gaoyali@spic.com.cn (Y.G.); liuyanbo@spic.com.cn (Y.L.)
2 Faculty of Automation and Information Engineering, Xi'an University of Technology, Xi'an 710048, China
3 State Key Discipline Laboratory of Wide Band Gap Semiconductor Tecchnology, Shaanxi Joint Key Laboratory of Graphene, School of Microelectronics, Xidian University, Xi'an 710071, China; zhoulongxdedu@163.com
* Correspondence: zhlin@xidian.edu.cn

Received: 15 December 2019; Accepted: 18 January 2020; Published: 2 February 2020

Abstract: Perovskite solar cell efficiency is not only related with material properties, but also affected by the interface engineering that used in perovskite solar cells. The perovskite film/electrode interface properties play important roles in charge carrier extraction, transport, and recombination. To achieve better interface contact for the device operation, proper interlayers or surface treatment should be applied. In this study, we applied a poly(3,4-ethylenedioxythiophene):poly(styrene sulfonate) (PEDOT:PSS) interlayer with a solvent/solution washing treatment as the hole transport layer. It showed that by the solvent/solution treatment, the PEDOT:PSS film conductivity was significantly enhanced, and hence, the charge carrier transfer efficiency was efficiently improved, and the device short-circuit current density was enlarged. Finally, the device efficiency significantly increased from 14.8% to 16.2%.

Keywords: perovskite solar cells; PEDOT:PSS; solvent dripping treatment; interface engineering

1. Introduction

The perovskite solar cell (PSC) has received significant attention because of their unique properties such as high power conversion efficiency, simple solution processibility, high balanced charge carrier mobility, and intense light absorption [1–9]. In the past few years, the highest device power conversion efficiency (PCE) has been rapidly increased from 3.8% up to over 24% [10–14], and this PCE can be further improved by applying proper interface engineering, solvent engineering and composition engineering approaches [5,15–28].

Commonly, in planar PSCs with p-i-n structure, the [6,6]-phenyl-C_{61}-butyric acid methyl ester (PCBM) layer is mostly used as the electron transport layer (ETL), and the poly(3,4-ethylenedioxythiophene):poly(styrene sulfonate) (PEDOT:PSS) layer was mostly employed as the hole transport layer (HTL). Moreover, the device based on this structure has achieved considerable performance [18,29,30]. Even so, ascribed to the acidic and hydrophilic nature of PEDOT:PSS interlayer, poor stability and inefficient charge extraction/collection have become the challenging issues. Hence, proper methods to enhance the PEDOT:PSS conductivity and hydrophobic properties or using inorganic NiO HTL to replace PEDOT:PSS film become more important [23,25,26,31–34].

Previously, in organic solar cells and perovskite solar cells, some polar solvents including ethylene glycol (EG), dimethyl sulfoxide (DMSO), dopamine, F4-TCNQ, dimethyl formamide (DMF), imidazole, etc. have been used as additives to enhance the PEDOT:PSS conductivity and tune the work-function [35–38]. Among them, DMSO exhibits superior advantages due to its good dielectric constant, dipolar moment, and relatively higher boiling point. Hence, between PEDOT:PSS and DMSO molecules, strong dipole-dipole or dipolar-charge interactions can be easily formed, which can enhance the film conductivity and charge carrier mobility. Previously, some studies have been performed to investigate the PEDOT:PSS work-function and morphology effects on the perovskite thin film morphologies and corresponding device performance [32,33,39,40]. Even though the DMSO has been widely used in perovskite solution precursor or as an additive in PEDOT:PSS solution, there are few researches about direct solvent treatment on PEDOT:PSS film to optimize film quality and device performance.

In this study, we studied the solvent/solution dripping effects on the PEDOT:PSS and perovskite film properties. By employing the solvent/solution washing treated PEDOT:PSS as HTL, high performance perovskite solar cell devices were achieved. The PCE was enhanced to 16.2% which was much higher than that of the device with pristine PEDOT:PSS film (14.8%). After a series of characterization measurements, it was found that the significantly increased device short circuit current density (J_{sc}) was due to the improved conductivity of the PEDOT:PSS film.

2. Results and Discussion

By spin coating the PEDOT:PSS precursors with different coating speeds, the pristine PEDOT:PSS films with different thicknesses were formed. It was surprised that the PEDOT:PSS thickness has a significant effect on the final device performance. From Figure 1 and Table 1, it can be found that the device open circuit voltage (V_{oc}) and J_{sc} significantly increased upon increasing the coating speed of PEDOT:PSS HTL. Hence, the efficiency of solar cell devices was enhanced. It is clear to see that the J_{sc} gradually increased upon increasing the coating speed, indicating that the enhanced shunt resistance/series resistance (R_{sh}/R_s) ratio and/or decreased device resistance upon decreasing the PEDOT:PSS layer thickness (Table 1). To further increase the device performance, enhancing the PEDOT:PSS layer conductivity is necessary, and moreover, to enable a large thickness range of the interlayer is beneficial for printed devices.

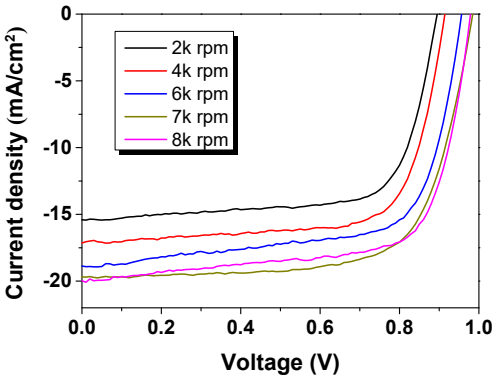

Figure 1. Current density–voltage (J–V) characteristics of perovskite solar cell (PSC) devices based on poly(3,4-ethylenedioxythiophene):poly(styrene sulfonate) (PEDOT:PSS) hole transport layer (HTL) with different coating speeds.

Table 1. Average device parameters of twelve PSCs based on different PEDOT:PSS coating conditions.

rpm	PEDOT:PSS Thickness	V_{oc} (V)	J_{sc} (mA/cm^2)	FF	PCE (%)
2000	62–68 nm	0.90 ± 0.02	15.40 ± 0.32	0.73 ± 0.03	10.1 ± 0.04
4000	46–49 nm	0.91 ± 0.02	17.16 ± 0.25	0.74 ± 0.03	11.6 ± 0.5
6000	34–38 nm	0.96 ± 0.01	18.82 ± 0.23	0.75 ± 0.02	13.5 ± 0.4
7000	26–30 nm	0.98 ± 0.01	19.80 ± 0.18	0.74 ± 0.02	14.4 ± 0.4
8000	24–28 nm	0.97 ± 0.01	19.64 ± 0.16	0.75 ± 0.02	14.3 ± 0.3

To improve the conductivity of PEDOT:PSS HTLs, a DMSO solvent treatment was taken during the PEDOT:PSS spin coating step. For the as-prepared PEDOT:PSS film (~30 nm) without solvent washing treatment, the conductivity was about 1.7×10^{-3} S cm^{-1} [34]. For the PEDOT:PSS film with DMSO solvent washing treatment, the conductivity increased to 0.7 S cm^{-1}, which is similar with the literature reported that the polar organic solvents could improve the PEDOT:PSS conductivity [32]. The conductivity enhancement mechanism has been reported previously [32]. Some PSS chains could be washed away from PEDOT:PSS films by DMSO solvent. Therefore, the ratio of PEDOT was increased, leading to higher conductivity.

With the DMSO solvent washing treatment, the PSS chains could be removed from PEDOT:PSS, which could be confirmed by XPS spectra (Escalab 250Xi, Thermo Scientific, Waltham, MA, USA). The S 2*p* has two states: one is from S in PSS (166–172 eV), and another one is from S atoms in PEDOT (162–166 eV). The ratio of S *sp* XPS intensity in PEDOT to that in PSS is significantly enhanced after treating with DMSO solvent (Figure 2) [41]. The relatively increased PEDOT ratio is contributed to the increased conductivity.

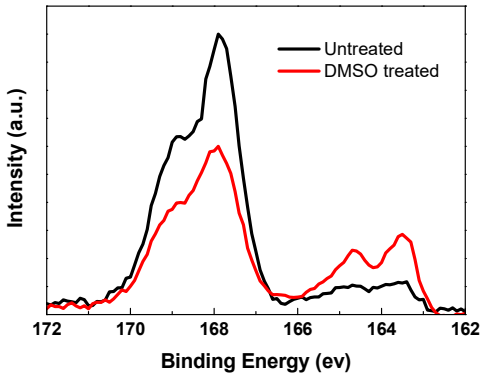

Figure 2. S 2*p* XPS spectra of PEDOT:PSS films without and with solvent washing treatment.

The effect of PSS chain removal from PEDOT:PSS on PEDOT:PSS film surface morphologies was investigated by atomic force microscopy (AFM) techniques (Dimension Icon AFM, Bruker, Billerica, MA, USA). Figure 3 shows the topography images of a 2×2 μm^2 area of pristine and DMSO solvent treated PEDOT:PSS films. The root mean square (RMS) roughness of pristine PEDOT:PSS thin film was 1.21 nm, indicating a quite smooth surface. After DMSO solvent washing treatment, crystal grains became clearer and the film surface became rougher, resulting in an increased root mean square (RMS) roughness of 2.92 nm. The increased RMS is mainly induced by the PSS chains removal and PEDOT chains aggregation. The increased conducting PEDOT-rich regions lead to superior charge-transport pathways for the treated films. Thus, the PEDOT:PSS film with solvent washing treatment exhibited higher conductivity.

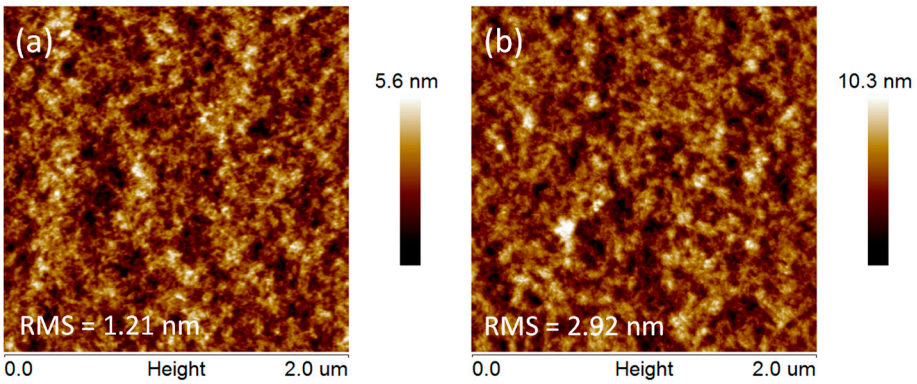

Figure 3. Atomic force microscopy (AFM) images of PEDOT:PSS films (**a**) without and (**b**) with DMSO solvent washing treatment.

The perovskite thin films deposited on pristine and DMSO solvent washing treated PEDOT:PSS were studied by scanning electron microscopy (SEM, JSM-7800F SEM, Japan). As exhibited in Figure 4, the perovskite film based on solvent washing treated PEDOT:PSS had similar crystal morphology with that of the perovskite film based on pristine PEDOT:PSS. All the perovskite films are uniform with large regular crystallites, and they fully cover the underlying layer. The favorable thin film uniformity and coverage indicate a homogenous nucleation of the perovskites on the substrates. The crystal size increased possibly due to the relatively hydrophobic nature of solvent washing treated PEDOT:PSS, which is beneficial for device performance [42]. In order to illustrate the effect of solvent treatment, we have measured the X-ray diffraction (XRD, Bruker D8 Advance XRD instrument, Billerica, MA, USA) and UV-Vis of the perovskites without or with solvent treatment. Figure 5a presents the UV-vis absorption spectra of perovskites and showed that the film with solvent washing treated PEDOT:PSS exhibited higher light absorption than pristine film. The thin film crystallinity was investigated by XRD, and the XRD patterns of perovskite films with/without solvent treatment are shown in Figure 5b. The diffraction peaks around 14.21°, 28.51°, and 31.88° are assigned to the (110), (220), and (310) crystal planes, respectively, which indicates that the perovskite film is formed with good quality. Meanwhile, the PbI_2 peak around 12.6° appeared, and the exceed PbI_2 could efficiently passivate the perovskite grain boundaries and reduce trap density as reported [16,43]. Moreover, the solvent washing treated PEDOT:PSS produced higher crystallinity of treated film than that of pristine film. This improved film crystallinity has positive effect on charge transport and charge extraction.

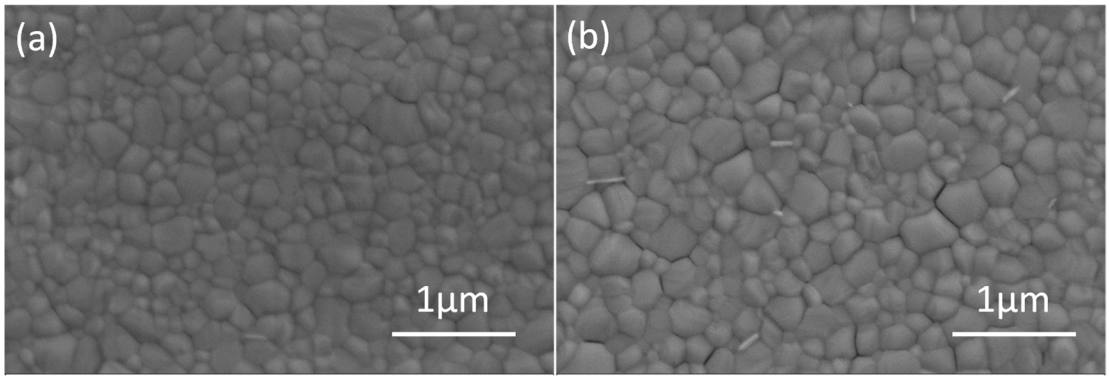

Figure 4. SEM images of (**a**) pristine and (**b**) DMSO solvent washing treated PEDOT:PSS based perovskite films.

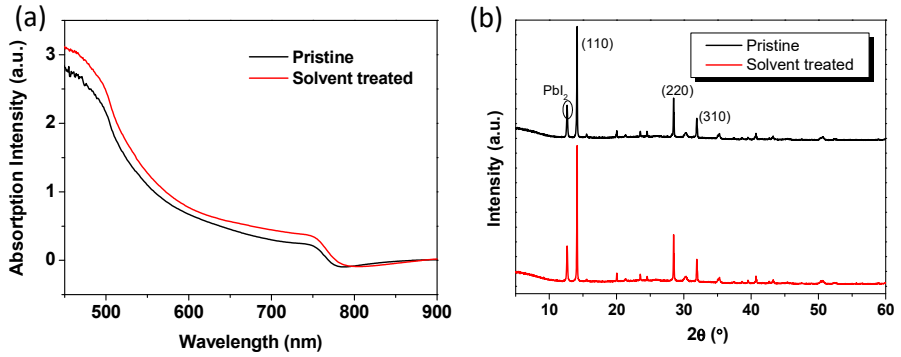

Figure 5. UV-vis and XRD spectra of (**a**) pristine and (**b**) DMSO solvent washing treated PEDOT:PSS based perovskite films.

The photoluminescence (PL) spectra of perovskite films based on pristine and solvent washing treated PEDOT:PSS were also studied (Figure 6a). Compared to pristine PEDOT:PSS based perovskite film, the solvent washing treated PEDOT:PSS based perovskite film exhibited more efficient PL quenching, indicating that charge transfer between solvent washing treated PEDOT:PSS and perovskite is more efficient. This is beneficial for efficient charge transfer and charge extraction. Time-resolved PL (TR-PL) measurement was also carried out to investigate the charge carrier dynamic behavior regarding to the solvent washing treatment. It can be seen that the average PL lifetime decreased from 47.4 ns to 36.7 ns (Table 2). The decreased PL lifetime indicates that an efficient charge transfer induced quenching process occurred based on solvent treatment.

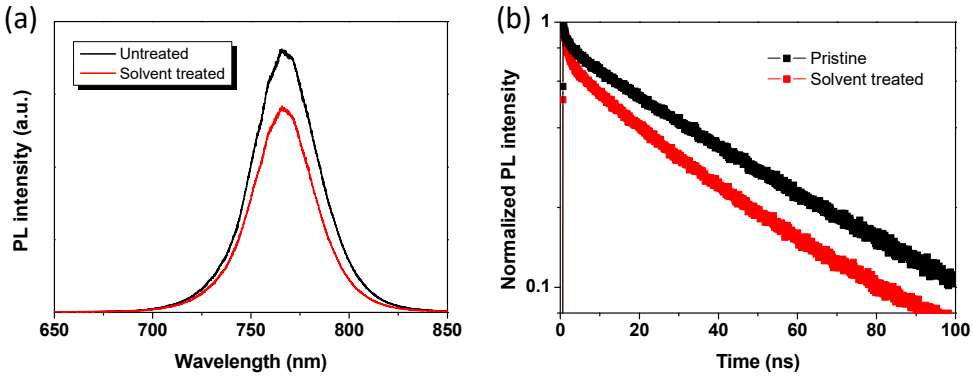

Figure 6. (**a**) Steady-state photoluminescence (PL) and (**b**) TR-PL spectra for perovskite films based on pristine and DMSO solvent washing treated PEDOT:PSS layers.

Table 2. Fitted decay times of perovskite films based on pristine and solvent washing treated PEDOT:PSS layers.

Conditions	A1	τ_1 (ns)	A2	τ_2 (ns)	τ_{ave} (ns)
Pristine	0.18	2.9	0.82	47.9	47.4
Solvent treated	0.23	2.1	0.77	37.3	36.7

The solvent washing treatment effect on perovskite solar cell performance was also studied as well. The device adopted a configuration of ITO/PEDOT:PSS/Perovskite/PCBM/BCP/Ag, and the perovskite layer was composed by MAI, PbI_2, and $PbCl_2$ (The details can be seen in Supplementary Materials) [44]. Table 3 summarizes the parameters of the devices, and Figure 7 exhibits the device current density–voltage (*J*–*V*) characteristics. The pristine PEDOT:PSS layer exhibited a J_{sc} of 19.8 mA/cm^2, a V_{oc} of 0.98 V, a fill factor (FF) of 0.76, and an overall PCE of 14.8%. After DMSO solvent washing treatment, the J_{sc} significantly increased to 22.6 mA/cm^2, V_{oc} had almost no change, and FF slightly decreased to 0.73. Hence, the overall PCE was enhanced to 16.2%. The performance

enhancement is mainly resulting from J_{sc} increment. The increased film conductivity and perovskite film absorption all contributed to the J_{sc} enhancement. This can be further confirmed by incident photon-to-electron conversion efficiency (IPCE) measurements. The DMSO solvent washing treated PEDOT:PSS based device showed improvement in IPCE spectra from 350 nm to 750 nm. This method is also applied to other solvent system like DMF. As shown in Table 1, the DMF dripping treatment improved the device PCE to 15.5% with an increased J_{sc} of 20.9 mA/cm^2.

Table 3. Average device parameters of twenty-four perovskite solar cells based on pristine and solvent washing treated PEDOT:PSS layers.

Interlayer	V_{oc} (V)	J_{sc} (mA/cm^2)	FF	PCE (%)	R_s (Ω cm^2)	R_{sh} (kΩ cm^2)
Pristine	0.98 ± 0.01	19.8 ± 0.2	0.76 ± 0.02	14.8 ± 0.2	4.2	1.5
DMSO dripping	0.98 ± 0.01	22.6 ± 0.4	0.73 ± 0.03	16.2 ± 0.3	2.1	1.1
DMF dripping	0.99 ± 0.01	20.9 ± 0.3	0.75 ± 0.02	15.5 ± 0.2	2.7	1.4

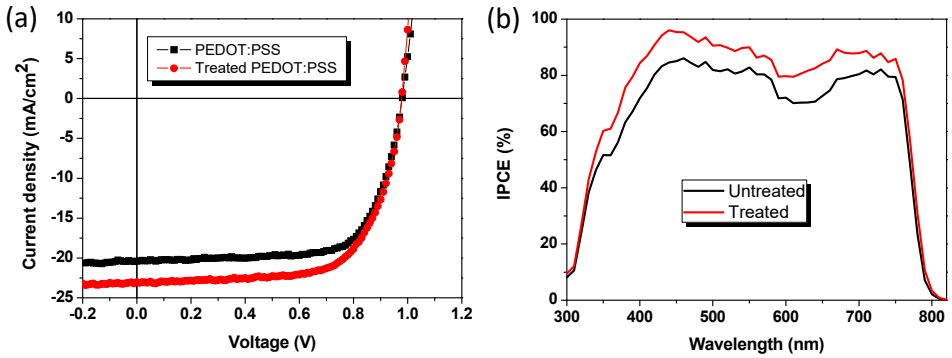

Figure 7. (**a**) *J*–*V* characteristics and (**b**) IPCE spectra of perovskite solar cells based on pristine and DMSO solvent washing treated PEDOT:PSS layers.

The device R_s and R_{sh} were extracted from the *J*–*V* curves to further understand the solvent washing treatment effects. As can be seen from Table 3, the device with pristine PEDOT:PSS had a R_s value of 4.2 Ω cm^2 and a R_{sh} value of 1.5 kΩ cm^2. After solvent washing treatment, R_s decreased to 2.1 Ω cm^2, while R_{sh} also decreased to 1.1 kΩ cm^2. The decrease in R_s is ascribed to the PEDOT:PSS conductivity enhancement [45]. While decreased R_{sh} is because of the rougher surface of PEDOT:PSS, which might increase the leakage current.

Hysteresis behaviors of different devices were also performed by measuring the *J*–*V* characteristics in both forward and reverse directions, as shown in Figure 8. Compared to pristine PEDOT:PSS based device, solvent washing treated device exhibited slightly larger hysteresis behavior which may be due to its rough surface caused by PEDOT chains aggregation and/or trapping/detrapping of charge carriers due to interface defects [32].

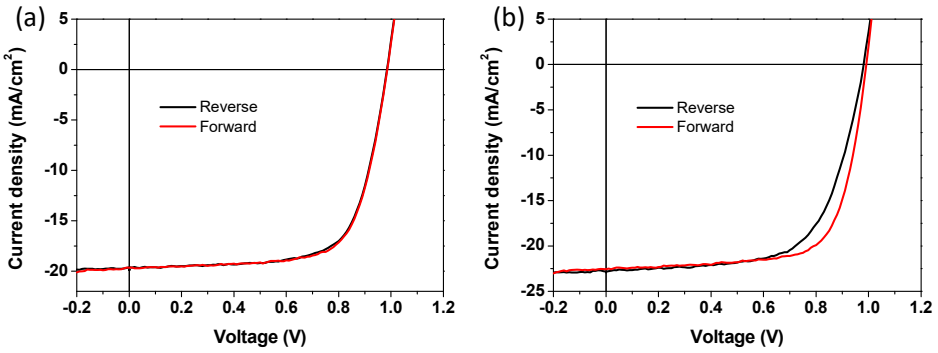

Figure 8. Hysteresis characteristics of perovskite solar cells based on pristine and DMSO solvent washing treated PEDOT:PSS layers.

3. Conclusions

In conclusion, we have studied the DMSO solvent washing treatment effect on the PEDOT:PSS film properties, perovskite film quality, and corresponding perovskite device performance. The results exhibited that the DMSO solvent washing treatment could significantly enhance the film conductivity, charge carrier transfer efficiency, and the quality of perovskite. Hence, devices with the treated PEDOT:PSS layer exhibited improved J_{sc} and PCE.

Supplementary Materials: The following are available online at http://www.mdpi.com/2079-6412/10/2/127/s1.

Author Contributions: Conceptualization, Z.L.; methodology, G.L., X.W.; validation, L.Z.; formal analysis, G.L., M.Z. and L.Z.; investigation, G.L., and Y.G.; data curation, G.L., X.W. and L.Z.; writing—original draft preparation, G.L.; writing—review and editing, Z.L., G.L. and L.Z.; visualization, M.Z., Y.G. and Y.L.; supervision, Z.L.; project administration, Z.L. All authors have read and agreed to the published version of the manuscript.

Funding: This research was funded by National Natural Science Foundation of China, grant number 61604119, 61704131, and 61804111, and the Fundamental Research Funds for the Central Universities.

Conflicts of Interest: The authors declare no conflict of interest.

References

1. Xing, G.; Mathews, N.; Sun, S.; Lim, S.S.; Lam, Y.M.; Grätzel, M.; Mhaisalkar, S.; Sum, T.C. Long-range balanced electron- and hole-transport lengths in organic-inorganic $CH_3NH_3PbI_3$. *Science* **2013**, *342*, 344–347. [CrossRef] [PubMed]
2. Shi, D.; Adinolfi, V.; Comin, R.; Yuan, M.; Alarousu, E.; Buin, A.; Chen, Y.; Hoogland, S.; Rothenberger, A.; Katsiev, K.; et al. Low trap-state density and long carrier diffusion in organolead trihalide perovskite single crystals. *Science* **2015**, *347*, 519–522. [CrossRef] [PubMed]
3. Dong, Q.; Fang, Y.; Shao, Y.; Mulligan, P.; Qiu, J.; Cao, L.; Huang, J. Electron-hole diffusion lengths > 175 μm in solution-grown $CH_3NH_3PbI_3$ single crystals. *Science* **2015**, *347*, 967–970. [CrossRef] [PubMed]
4. Stranks, S.D.; Eperon, G.E.; Grancini, G.; Menelaou, C.; Alcocer, M.J.P.; Leijtens, T.; Herz, L.M.; Petrozza, A.; Snaith, H.J. Electron-hole diffusion lengths exceeding 1 micrometer in an organometal trihalide perovskite absorber. *Science* **2013**, *342*, 341–344. [CrossRef]
5. Chang, J.; Zhu, H.; Li, B.; Isikgor, F.H.; Hao, Y.; Xu, Q.; Ouyang, J. Boosting the performance of planar heterojunction perovskite solar cell by controlling the precursor purity of perovskite materials. *J. Mater. Chem. A* **2016**, *4*, 887–893. [CrossRef]
6. Xiao, J.; Chang, J.; Li, B.; Isikgor, F.H.; Wang, D.; Fan, Z.; Lin, Z.; Ouyang, J.; Zeng, K.; Chen, J. Room temperature ferroelectricity of hybrid organic–inorganic perovskites with mixed iodine and bromine. *J. Mater. Chem. A* **2018**, *6*, 9665–9676. [CrossRef]
7. Chang, J.; Xiao, J.; Lin, Z.; Zhu, H.; Xu, Q.-H.; Zeng, K.; Hao, Y.; Ouyang, J. Elucidating the charge carrier transport and extraction in planar heterojunction perovskite solar cells by Kelvin probe force microscopy. *J. Mater. Chem. A* **2016**, *4*, 17464–17472. [CrossRef]
8. Su, J.; Zhang, Z.; Hou, J.; Liu, M.; Lin, Z.; Hu, Z.; Chang, J.; Hao, Y. Pressure-dependent mechanical and thermal properties of lead-free halide double perovskite $Cs_2AgB''X_6$ (B″ = In, Bi; X = Cl, Br, I). *Adv. Theory Simul.* **2019**, *2*, 1900164. [CrossRef]
9. Zhang, Z.; Su, J.; Hou, J.; Lin, Z.; Hu, Z.; Chang, J.; Zhang, J.; Hao, Y. Potential applications of halide double perovskite Cs_2AgInX_6 (X = Cl, Br) in flexible optoelectronics: Unusual effects of uniaxial strains. *J. Phys. Chem. Lett.* **2019**, *10*, 1120–1125. [CrossRef]
10. Chiang, C.-H.; Nazeeruddin, M.K.; Grätzel, M.; Wu, C.-G. The synergistic effect of H_2O and DMF towards stable and 20% efficiency inverted perovskite solar cells. *Energy Environ. Sci.* **2017**, *10*, 808–817. [CrossRef]
11. Bi, D.; Yi, C.; Luo, J.; Décoppet, J.D.; Zhang, F.; Zakeeruddin, S.M.; Li, X.; Hagfeldt, A.; Grätzel, M. Polymer-templated nucleation and crystal growth of perovskite films for solar cells with efficiency greater than 21%. *Nat. Energy* **2016**, *1*, 16142. [CrossRef]
12. Zhou, L.; Lin, Z.; Ning, Z.; Li, T.; Guo, X.; Ma, J.; Su, J.; Zhang, C.; Zhang, J.; Liu, S.; et al. Highly efficient and stable planar perovskite solar cells with modulated diffusion passivation toward high power conversion efficiency and ultrahigh fill factor. *Sol. RRL* **2019**, 1900293. [CrossRef]

13. Zhao, P.; Feng, L.; Lin, Z.; Wang, J.; Su, J.; Hu, Z.; Zhang, J.; Ouyang, X.; Chang, J.; Hao, Y. Theoretical analysis of two-terminal and four-terminal perovskite/CIGS tandem solar cells. *Sol. RRL* **2019**, 1900303. [CrossRef]
14. Zhao, P.; Yue, M.; Lei, C.; Lin, Z.; Su, J.; Chen, D.; Zhang, C.; Zhang, J.; Chang, J.; Hao, Y. Device simulation of organic–inorganic halide perovskite/crystalline silicon four-terminal tandem solar cell with various antireflection materials. *IEEE J. Photovolt.* **2018**, *8*, 1685–1691. [CrossRef]
15. Ma, J.; Su, J.; Lin, Z.; Zhou, L.; He, J.; Zhang, J.; Liu, S.; Chang, J.; Hao, Y. Improve the oxide/perovskite heterojunction contact for low temperature high efficiency and stable all-inorganic CsPbI2Br perovskite solar cells. *Nano Energy* **2020**, *67*, 104241. [CrossRef]
16. Chang, J.; Zhu, H.; Xiao, J.; Isikgor, F.H.; Lin, Z.; Hao, Y.; Zeng, K.; Xu, Q.-H.; Ouyang, J. Enhancing the planar heterojunction perovskite solar cell performance through tuning the precursor ratio. *J. Mater. Chem. A* **2016**, *4*, 7943–7949. [CrossRef]
17. Chang, J.; Lin, Z.; Zhu, H.; Isikgor, F.H.; Xu, Q.-H.; Zhang, C.; Hao, Y.; Ouyang, J. Enhancing the photovoltaic performance of planar heterojunction perovskite solar cells by doping the perovskite layer with alkali metal ions. *J. Mater. Chem. A* **2016**, *4*, 16546–16552. [CrossRef]
18. Ma, J.; Lin, Z.; Guo, X.; He, J.; Hu, Z.; Su, J.; Zhang, J.; Chang, J.; Hao, Y. Low temperature ZnO/TiO*x* electron-transport layer processed from aqueous solution for highly efficient and stable planar perovskite solar cells. *Mater. Today Energy* **2019**, *14*, 100351. [CrossRef]
19. Jeon, N.J.; Noh, J.H.; Yang, W.S.; Kim, Y.C.; Ryu, S.; Seo, J.; Seok, S. Il Compositional engineering of perovskite materials for high-performance solar cells. *Nature* **2015**, *517*, 476–480. [CrossRef]
20. Jeon, N.J.; Noh, J.H.; Kim, Y.C.; Yang, W.S.; Ryu, S.; Seok, S. Il Solvent engineering for high-performance inorganic-organic hybrid perovskite solar cells. *Nat. Mater.* **2014**, *13*, 897–903. [CrossRef]
21. Huang, X.; Du, J.; Guo, X.; Lin, Z.; Ma, J.; Su, J.; Feng, L.; Zhang, C.; Zhang, J.; Chang, J.; et al. Polyelectrolyte-doped SnO_2 as a tunable electron transport layer for high-efficiency and stable perovskite solar cells. *Sol. RRL* **2020**, *4*, 1900336. [CrossRef]
22. Lin, Z.; Chang, J.; Zhu, H.; Xu, Q.-H.; Zhang, C.; Ouyang, J.; Hao, Y. Enhanced planar heterojunction perovskite solar cell performance and stability using PDDA polyelectrolyte capping agent. *Sol. Energy Mater. Sol. Cells* **2017**, *172*, 133–139. [CrossRef]
23. Liu, Z.; Chang, J.; Lin, Z.; Zhou, L.; Yang, Z.; Chen, D.; Zhang, C.; Liu, S.F.; Hao, Y. High-performance planar perovskite solar cells using low temperature, solution-combustion-based nickel oxide hole transporting layer with efficiency exceeding 20%. *Adv. Energy Mater.* **2018**, *8*, 1703432. [CrossRef]
24. Ma, J.; Lin, Z.; Guo, X.; Zhou, L.; Su, J.; Zhang, C.; Yang, Z.; Chang, J.; (Frank) Liu, S.; Hao, Y. Low-temperature solution—Processed ZnO electron transport layer for highly efficient and stable planar perovskite solar cells with efficiency over 20%. *Sol. RRL* **2019**, *3*, 1900096. [CrossRef]
25. Wang, S.; Zhang, B.; Feng, D.; Lin, Z.; Zhang, J.; Hao, Y.; Fan, X.; Chang, J. Achieving high performance and stable inverted planar perovskite solar cells using lithium and cobalt co-doped nickel oxide as hole transport layers. *J. Mater. Chem. C* **2019**, *7*, 9270–9277. [CrossRef]
26. Zhang, S.; Su, J.; Lin, Z.; Tian, K.; Guo, X.; Zhang, J.; Chang, J.; Hao, Y. Beneficial role of organolead halide perovskite CH_3 NH_3 PbI_3/SnO_2 interface: Theoretical and experimental study. *Adv. Mater. Interfaces* **2019**, *6*, 1900400. [CrossRef]
27. Guo, X.; Lin, Z.; Ma, J.; Hu, Z.; Su, J.; Zhang, C.; Zhang, J.; Chang, J.; Hao, Y. Low temperature combustion synthesized indium oxide electron transport layer for high performance and stable perovskite solar cells. *J. Power Sources* **2019**, *438*, 226981. [CrossRef]
28. Zhou, L.; Guo, X.; Lin, Z.; Ma, J.; Su, J.; Hu, Z.; Zhang, C.; Liu, S.F.; Chang, J.; Hao, Y. Interface engineering of low temperature processed all-inorganic CsPbI2Br perovskite solar cells toward PCE exceeding 14%. *Nano Energy* **2019**, *60*, 583–590. [CrossRef]
29. Xu, J.; Buin, A.; Ip, A.H.; Li, W.; Voznyy, O.; Comin, R.; Yuan, M.; Jeon, S.; Ning, Z.; McDowell, J.J.; et al. Perovskite-fullerene hybrid materials suppress hysteresis in planar diodes. *Nat. Commun.* **2015**, *6*, 7081. [CrossRef]
30. Shao, Y.; Xiao, Z.; Bi, C.; Yuan, Y.; Huang, J. Origin and elimination of photocurrent hysteresis by fullerene passivation in $CH_3NH_3PbI_3$ planar heterojunction solar cells. *Nat. Commun.* **2014**, *5*, 5784. [CrossRef]
31. You, J.; Meng, L.; Song, T.-B.; Guo, T.-F.; Yang, Y.M.; Chang, W.-H.; Hong, Z.; Chen, H.; Zhou, H.; Chen, Q.; et al. Improved air stability of perovskite solar cells via solution-processed metal oxide transport layers. *Nat. Nanotechnol.* **2015**, *11*, 75–81. [CrossRef] [PubMed]

32. Xia, Y.; Sun, K.; Chang, J.; Ouyang, J. Effects of organic inorganic hybrid perovskite materials on the electronic properties and morphology of poly(3,4-ethylenedioxythiophene): Poly(styrenesulfonate) and the photovoltaic performance of planar perovskite solar cells. *J. Mater. Chem. A* **2015**, *3*, 15897–15904. [CrossRef]
33. Wang, Q.; Chueh, C.-C.; Eslamian, M.; Jen, A.K.-Y. Modulation of PEDOT:PSS pH for efficient inverted perovskite solar cells with reduced potential loss and enhanced stability. *ACS Appl. Mater. Interfaces* **2016**, *8*, 32068–32076. [CrossRef] [PubMed]
34. Lin, Z.; Zhou, J.; Zhou, L.; Wang, K.; Li, W.; Su, J.; Hao, Y.; Li, Y.; Chang, J. Simultaneously enhanced performance and stability of inverted perovskite solar cells via a rational design of hole transport layer. *Org. Electron.* **2019**, *73*, 69–75. [CrossRef]
35. Tan, L.; Zhou, H.; Ji, T.; Huang, L.; Chen, Y. High conductive PEDOT via post-treatment by halobenzoic for high-efficiency ITO-free and transporting layer-free organic solar cells. *Org. Electron.* **2016**, *33*, 316–323. [CrossRef]
36. Thomas, J.P.; Zhao, L.; McGillivray, D.; Leung, K.T. High-efficiency hybrid solar cells by nanostructural modification in PEDOT:PSS with co-solvent addition. *J. Mater. Chem. A* **2014**, *2*, 2383. [CrossRef]
37. Li, X.-Y.; Zhang, L.; Tang, F.; Bao, Z.; Lin, J.; Li, Y.; Chen, L.; Ma, C. The solvent treatment effect of the PEDOT:PSS anode interlayer in inverted planar perovskite solar cells. *RSC Adv.* **2016**, *6*, 24501–24507. [CrossRef]
38. Prosa, M.; Tessarolo, M.; Bolognesi, M.; Cramer, T.; Chen, Z.; Facchetti, A.; Fraboni, B.; Seri, M.; Ruani, G.; Muccini, M. Efficient and versatile interconnection layer by solvent treatment of PEDOT:PSS interlayer for air-processed organic tandem solar cells. *Adv. Mater. Interfaces* **2016**, *3*, 1600770. [CrossRef]
39. Adam, G.; Kaltenbrunner, M.; Głowacki, E.D.; Apaydin, D.H.; White, M.S.; Heilbrunner, H.; Tombe, S.; Stadler, P.; Ernecker, B.; Klampfl, C.W.; et al. Solution processed perovskite solar cells using highly conductive PEDOT:PSS interfacial layer. *Sol. Energy Mater. Sol. Cells* **2016**, *157*, 318–325. [CrossRef]
40. Liu, D.; Li, Y.; Yuan, J.; Hong, Q.; Shi, G.; Yuan, D.; Wei, J.; Huang, C.; Tang, J.; Fung, M.-K. Improved performance of inverted planar perovskite solar cells with F4-TCNQ doped PEDOT:PSS hole transport layers. *J. Mater. Chem. A* **2017**, *5*, 5701–5708. [CrossRef]
41. Xia, Y.; Ouyang, J. PEDOT:PSS films with significantly enhanced conductivities induced by preferential solvation with cosolvents and their application in polymer photovoltaic cells. *J. Mater. Chem.* **2011**, *21*, 4927. [CrossRef]
42. Bi, C.; Wang, Q.; Shao, Y.; Yuan, Y.; Xiao, Z.; Huang, J. Non-wetting surface-driven high-aspect-ratio crystalline grain growth for efficient hybrid perovskite solar cells. *Nat. Commun.* **2015**, *6*, 7747. [CrossRef] [PubMed]
43. Chen, Q.; Zhou, H.; Song, T.-B.; Luo, S.; Hong, Z.; Duan, H.-S.; Dou, L.; Liu, Y.; Yang, Y. Controllable self-induced passivation of hybrid lead iodide perovskites toward high performance solar cells. *Nano Lett.* **2014**, *14*, 4158–4163. [CrossRef] [PubMed]
44. Zhou, L.; Chang, J.; Liu, Z.; Sun, X.; Lin, Z.; Chen, D.; Zhang, C.; Zhang, J.; Hao, Y. Enhanced planar perovskite solar cell efficiency and stability using a perovskite/PCBM heterojunction formed in one step. *Nanoscale* **2018**, *10*, 3053–3059. [CrossRef]
45. Lin, Z.; Chang, J.; Xiao, J.; Zhu, H.; Xu, Q.-H.; Zhang, C.; Ouyang, J.; Hao, Y. Interface studies of the planar heterojunction perovskite solar cells. *Sol. Energy Mater. Sol. Cells* **2016**, *157*, 783–790. [CrossRef]